The rates of different core collapse supernovae in the Palomar Transient Factory From Core-Collapse to Superluminous: The rates of massive star explosions across all luminosity scales in the Palomar Transient Factory

C. Frohmaier,[1]⋆C. R. Angus,[2]†, M. Vincenzi[1] and M. Sullivan[2]

[1]*Institute of Cosmology and Gravitation, University of Portsmouth, Portsmouth, PO1 3FX, UK*
[2]*Department of Physics and Astronomy, University of Southampton, Highfield, Southampton, SO17 1BJ, UK*

ABSTRACT

We present the volumetric rates of core-collapse supernovae (CCSNe) and Type I superluminous supernove (SLSNe-I) discovered by the Palomar Transient Factory (PTF). We separated the PTF survey operations into several sub-survyes of regular cadence and high spectroscopic classification efficiency to obtain a high-quality, low redshift (z≤0.035) sample of 86 CC events. These sub-surveys were then replicated in a Monte-Carlo simulation involving hundreds of millions of CCSNe template realisations to forward-model the volumetric rate to infer the intrisic CCSN rate that best matched the PTF observations. From this, the CCSN rate was found to be $r_v^{\mathrm{CC}} = 9.10^{+1.55}_{-1.27} \times 10^{-5}$ SNe yr^{-1} Mpc^{-3} h_{70}^3. We performed an additional simulation on the sub-sample of 26 events classified as stripped-envelope supernovae (SESNe) and calculated the first direct measurement of the volumetric rate of SESNe to be $r_v^{\mathrm{SE}} = 2.41^{+0.8}_{-0.64} \times 10^{-5}$ SNe yr^{-1} Mpc^{-3} h_{70}^3. Our 10 SLSNe-I (z≤0.2) were identified from a literature sample of PTF events and the forward-modelling of their rate was performed on a whole-sky simulation. We found the volumetric rate to be $r_v^{\mathrm{SLSN-I}} = 49^{+30}_{-16}$ SNe yr^{-1}Gpc^{-3} h_{70}^3, which represents the most precise SLSNe-I rate measurement to-date. A simple cosmic star-formation history was normalized to each SN rate to compare their realtive frequency. We find that the local fraction of SLSN-I to SESN is ∼ 1/620 and the fraction of SLSN-I to all CCSN types is ∼ 1/2500.

Key words: keyword1 – keyword2 – keyword3

1 INTRODUCTION

***Apologies...I'm too lazy to add proper references at the moment so they're just commented**
Things to add:

• Importance of understanding rates of SESN (binary vs massive stars)

• One way to test similarity of progenitors this is to estimate the rates of these two classes of event - if they're similar this may suggest similar progenitors

• "This paper presents the first (?) direct measurement of the SESN rate at low-redshift alongside the best constrained low-z SLSN rate measurement such that we may begin to probe the respective populations of SNe which produce these events"

With the movement of transient surveys towards more wide-field, high cadence, untargeted surveys, we uncovering an increasing diversity in properties attributed to nominally 'normal'classes of SNe. This is perhaps most pronounced amongst the subclasses of Hydrogen-poor SNe which arise from massive stellar deaths (so called classes of 'stripped-envelope' SNe). Thought to originate from stars lacking in a helium and/or hydrogen envelope at the time of explosion, they can be further segregated into additional subclasses based upon their spectroscopic properties (such as the presence or absence of helium and width of spectral lines) into SNe Ib, Ic and Ic-BL (see [REFS] for a more detailed overview of SESN taxonomy). These SN classes are incredibly heterogeneous in nature [REFS], although can be broadly grouped based upon the relative abundances of H/He in their spectra. The differences in subtypes are typically attributed to variation in the mass of stellar envelope surrounding the progenitor at the point of explosion (whereby SNe IIb are partially stripped of their hydrogen, SNe Ib progenitors are fully stripped of any hydrogen envelopes, and SNe Ic progenitors are completely stripped of both their hydrogen and helium envelopes) [REFS].

⋆ E-mail: chris.frohmaier@port.ac.uk
† E-mail:

Though attributed to massive stellar collapse, the progenitor systems of SESNe are still unknown. The removal of a massive stellar envelope may take place through one of two main channels; either through gradual mass-loss via line-driven stellar winds, or through interaction with a binary companion. Direct searches for SESN progenitors either through pre-explosion imaging or colour excess in post-explosion images have yielded mixed results. A handful of hydrogen-rich SESN progenitors have been identified (e.g. SN 1993J, SN 2008ax, SN2011dh, SN2013df and SN2016gkg (Aldering et al. 1994; Smartt 2009,Crockett et al. 2008; Arcavi et al. 2011; Folatelli et al. 2015,Maund et al. 2011, Van Dyk et al. 2014, Kilpatrick et al. 2017; Tartaglia et al. 2017), leading to progenitor mass estimates M_{ZAMS} <20$M_\odot$, but for hydrogen-poor events, this task is less trivial, as they may originate from massive Wolf-Rayet stars which are most luminous at UV wavelengths, making them difficult to detect in optical imaging (Smartt 2009; Eldridge et al. 2013). In the absence of a direct progenitor detection for hydrogen-poor SESNe, it is not clear whether the production of all SESNe occurs through one channel, or whether multiple progenitor channels are at play.

Recently an additional subclass of SESNe has emerged, hydrogen-poor Superluminous Supernovae (SLSNe-I. This growing subclass of SNe exhibit typically bright peak luminosities ($M \sim -20$) and long-lived optical light curves, requiring extreme energies behind their production (events frequently radiate in excess of $\sim 10^{51}$ ergs s^{-1}), make them some of the most extreme optical transients to be identified within modern surveys, often detectable out to high redshift (??). Spectroscopically these events are blue and rather featureless prior to maximum light, with characteristic broad Oii ʌbsorption lines Quimby et al. 2011 and some stronger absorption features in the near ultraviolet (UV) attributed to heavy elements (see more detailed discussion in Quimby et al. 2018). However, at 30 rest-frame days post-max, the spectra of SLSNe-I more closely resemble both normal and broad-lined type Ic SNe at peak (Pastorello et al. 2010; Liu et al. 2017).

Here too, there exists significant uncertainty surrounding their progenitor systems, as their energy requirements surpass the typical energies produced under standard core-collapse models. Proposed models for their production range from interaction with hydrogen-free circumstellar material (???), to pair instability explosions (??), to energy injection from a central compact object (???). The latter of these theories, implemented through the spin down of a newly formed magnetar, is capable of broadly replicating the light curve evolution and spectroscopic features of a large number of SLSNe-I reasonably well (?????), although it is at present uncertain whether this mechanism alone can power SLSNe-I events, or if additional sources of energy are also required to fully encapsulate their physical properties [REFS].

In more recent years homogeneously selected samples of SLSNe have begun to highlight significant diversity in both their photometric and spectroscopic properties [De Cia 2018, Lunnan 2018, Angus 2019, Quimby 2019], demonstrating a much broader range of luminosities and evolutionary timescales than had been previously attributed to this spectroscopic class. Indeed, such samples have begun to expand the faint tail of the SLSN luminosity function, highlighting a potentially undersampled population of less luminous events in this spectroscopic class. The luminosities and energies associated with these less luminous SLSNe are much closer to those associated with SN Ia explosions, and draw nearer to the brighter end of a normal CCSN regime.

When combined with the propensity of these events to possess similar spectral features to Ic-BL SNe at late times and during the

nebular phase (Nicholl et al. 2016b; Jerkstrand et al. 2017), this has led to several suggestions that the two spectroscopic classes are perhaps connected. Additionally both events exhibit a similar preference in host environments, frequently occurring in low-luminosity, metal-poor star-forming galaxies [(e.g. Stanek et al. 2006; Chen et al. 2015; Perley et al. 2016b; Japelj et al. 2016; Perley et al. 2016a)].Given the connection of SNe Ic-BL with Long Gamma Ray Bursts (LGRBs) [(e.g. Stanek et al. 2003; Hjorth et al. 2003; Woosley & Bloom 2006; Modjaz et al. 2016)], events for which relativistic jets responsible for powering the LGRB also could be produced via magnetar spin-down [(e.g., Usov 1992; Wheeler et al. 2000; Thompson et al. 2004; Metzger et al. 2011)], which hints that perhaps there is some common underlying progenitor population responsible for producing these events.

SESNe, on the otherhand

SLSNe-I are intrinsically rare events, with an estimated rate of 0.001% of the core-collapse SN (CCSN) rate in the local Universe (???), which ostensibly increases with redshift, following trends in the cosmic star formation history (???). Understanding how the volumetric rate of SLSNe-I evolves with redshift will not only improve searches for them in both current and upcoming surveys such as Euclid and the Large Synoptic Survey Telescope (??), but can also help provide a better understanding of their likely progenitor systems. For instance, if SLSNe-I are associated with the formation of massive stars, their estimated rate should match the observable fraction of the stellar mass function occupied by stars of a given mass. Volumetric rates may also reflect any environmental dependencies in SLSN-I progenitor production. An evolving rate with redshift may reflect an evolution of host galaxy properties (such as metallicity or star formation rate) with cosmic time, and thus provide telling clues as to the dependencies of SLSN-I progenitors upon their host environment. Conversely, deviations from any expected environmental evolution at low/high redshift may reflect additional factors in progenitor production which may have previously been overlooked.

In this paper, we present the SLSN-I rate from the Palomar Transient Factory (PTF; ?). PTF was an automated optical sky transient survey operating at the Samuel Oschin 48 inch telescope (P48) at the Palomar Observatory, searching over 8000 deg^2 of the optical sky over its initial phase between 2009-2012, reaching typical depths of $M_R \sim$XX. This wide-field survey presents the perfect opportunity to constrain the low-redshift rate of SLSNe events, from which we may test the dependencies of SLSNe production in the Local Universe.

In Section 2 we begin with a description of the general method for calulating volumetric transient rates int he PTF survey. In Section 3 we present our template light curves and justify our assumptions for the model parameters. In Section 4 we describe our method of constructing the survey simulation and the construction of a supernova sample for each of our transient sub-types. This is followed by a detailed explanation of the marriage between simulation and observation to calculate the rates of our SN population. We conclude by reviewing the implications of our results in Section 5. Throughout, where relevant we assume a flat ΛCDM Universe with a matter density $\Omega_M = 0.3$ and a Hubble constant of $H_0 = 70$km s^1 Mpc^1, and we work in the AB photometric system.

2   RATES FROM THE PTF SURVEY

In this Section we detail the challenges faced when determining transient rates from survey data and outline our rate calculation method

for PTF. No sky survey discovers transients with 100 per cent efficiency and compensating for missed events is more complex than simply correcting for the Malmquist bias. Some factors affecting the performance of the survey, such as the cadence, are easily quantifiable, while other effects, such as adverse weather conditions vary in severity and are much more difficult to compensate for. These observational intricacies are often conflated with the intrinsic properties of the transient events themselves, for example, rapidly evolving transients are far more likely to be missed in low-cadence surveys. The PTF survey is not exempt from these complications, and in many circumstances they are only enhanced as the survey covered a wide-area with multiple cadence experiments (**?**). Throughout this work we extensively use the detection efficiencies of **?** to provide a statistical description of the single-epoch transient recovery efficiency. **?** inserted around 7 million artificial point sources into real PTF images to test the performance of the PTF transient detection pipeline. They found that a combination of the observing conditions (seeing/image quality, sky brightness, and limiting magnitude), the transient's host galaxy surface brightness, and the transient's magnitude provided a good description of the survey's performance. From this, a multidimensional efficiency grid was created that described the probability that a point source (in an arbitrary environment) would have been detected in PTF difference imaging at any point in the survey.

Our method, therefore, follows a simple prescription with SN light curve and host properties drawn from an arbitrary distribution and combined with the nightly observing conditions for PTF. Using the detection efficiencies of **?** we are able to make a probabilistic statement on whether each epoch on the light curve would have been detected in a PTF pointing. Performing a Monte-Carlo simulation of light curve realisations creates a complete description of the survey's performance as a function of the target SN population properties. At this stage the details of the SN simulations can follow two paths; (i) an "efficiency-based" approach to weight the individual SNe in the observed population (e.g. **??**), or (ii) a large Monte-Carlo simulation to forward-model the PTF survey to match realisations of an intrinsic SN rate with the observed SN populations (e.g. **??**). We considered the "efficiency-based" method, but found it inadequate for our study as it is typically used in well-controlled surveys for objects with a well-defined model parameter-space to simulate from (e.g. SNe Ia).

Given the recent advancements in CCSNe templates (**?**) and superluminous template modelling (**??**) (Check the SLSN citations please)we adopted the forward-modelling approach for our rates analysis and detail our method here. A key aspect of constructing the simulation is to treat both the real and simulated objects identically. Any choices we make regarding fixed volumes or observing strategy, therefore, must be universally applicable within PTF's operation and our simualtion. We first define an area, Θ, on the sky in which to perform our Monte-Carlo simulation and also choose an appropriate observing duration over which PTF would have been sensitive to our SNe of interest. There are subtle differences in the treatment of the observing area and time for the CCSNe and SLSNe, these differences are explained in Section XX and XX respectively. Since we are calculating volumetric rates, we also define a maximum distance out to which we can be confident PTF could observe our supernovae of interest. This is not only set by the maximum brightness of a typical object in the population, but also by the evolution of the light curve so that a sufficiently large number of observations for us to be confident of discovery. Again, the treatment of the maximum distance for each of our supernova population differs and is described in their relevant Sections.

Our simulations preceded under the follwoing methodology.

We first draw a random value for the assumed intrinsic volumetric rate (r_{input}). This is used to generate a number of corresponding events, N_{input}, that would have occurred in any set volume (V_{obs}) and observing duration (T_{obs}) drawn from the Poisson distribution

$$P(N_{input}; \lambda) = \frac{\lambda^{N_{input}} e^{-\lambda}}{N_{input}!} \tag{1}$$

where $\lambda = r_{input} T_{obs} V_{obs}$, and

$$V_{obs} = \frac{\Theta_{obs}}{41253} \frac{4\pi}{3} \left[\frac{c}{H_0} \int_0^z \frac{dz'}{\sqrt{\Omega_M (1+z')^3 + \Omega_\Lambda}} \right]^3 \text{Mpc}^3, \tag{2}$$

with the speed of light, c, Ω_M, Ω_Λ, and H_0 taking standard values.

Each object in the N_{input} sample is then assigned an explosion date, sky position, and a redshift such that they occur randomly and uniformly in the simulated volume-time space. The light curve properties for the N_{input} templates are drawn from a distribution of intrinsic population parameters described in Section XX and XY.

The next stage of simulation involves mock observations of our template SNe. For this we adopt the observational efficiencies from **?** to determine whether an object would have been detected by the PTF transient detection pipeline. Our simulation executes the observing strategy of PTF and rolls though the three years of operation. Each time an artificial SN falls within an observation we use the template's brightness on that epoch, along with the night's observing conditions, to make a probabilistic statement about whether that object would have been detected (an example for Type Ia SNe is presented in **?**). We require that our SN must have been 'detected' on at least 4 separate nights over our light curve template's duration, at which point we are confident a real object matching these requirements object would have obtained a spectroscopic classification. The total number of objects passing this detection criteria, N_{output} is obtained and represents the output for a single realisation of our rate simulation. Repeating this process many hundreds of thousands of times builds up a description of the relationship between the intrinsic supernova rate and the observed number of supernovae in the final sample. It is than a case of comparing the N_{output} SNe to the observed populations of real SNe, this then links back to the original distributions of r_{input} and, hence, the true SN rate.

It is apparent that this method heavily relies on a realistic SN template light curve in order to produce realiable output statistics. In the next section, therefore, we describe the SN templates used within our simulations.

Note to myself. We can be resaonably sure that the sample is complete because De Cia say they are not significantly biased in their sample (Section 2), considering we make quite a conservative redshift cut, we are can be confident our SLSN-I sample is complete.

3 SUPERNOVA TEMPLATE LIGHT CURVE

It would be great if Maria could add to this section

3.1   Type II Supernovae

3.1.1   PTF Sample

3.1.2   Templates

3.2   Stripped Envelope Supernovae

3.2.1   PTF Sample

3.2.2   Templates

To simulate the observable SESNe population in the PTF survey, we use the published core-collapse SN (CCSN) templates of Vincenzi et al. 2019, utilizing the 13 SN Ib, 7 SN Ic and 6 SN Ic-BL templates in the database. These bolometric templates typically extended between -10 and +150 from the peak, and provide daily sampled and de-reddened, rest-frame spectrophotometric evolution for each SN. These templates are then redshifted and a random host galaxy extinction applied **[DO WE DO THIS?]** before being inserted into the simulation.

3.3   Superluminous Supernovae

3.3.1   PTF Sample

3.3.2   Low-redshift SLSN-I Sample

To avoid any possible redshift evolutionary effects tied to the progenitor systems, we model the range of possible magnetar properties our template SLSNe-I may take based upon the magnetar properties attributed to a low-redshift sample of SLSNe events. As literature samples of SLSNe below our rate redshift range ($z < 0.2$) are relatively small, we expand our sample to include events below $z = 0.3$, thus ensuring a larger sample to define our parameter space.

For fitting the magnetar model to our SLSNe-I light curves, we place the following data restrictions upon our sample to guarantee adequate sampling across both the duration of the light curve and the underlying spectral energy distribution (SED) for each event:

(i) The existing light curves must have data in >3 separate photometric bands for better constraining the underlying SED.

(ii) The light curve must be well sampled in these bands (we require >6 epochs of data in each band across the observed duration of the event).

We then use Gaussian Processes to interpolate the SLSNe-I light curves. We then fit the resulting interpolated light curves with the phase dependent UV-absorbed blackbody model presented within **?** and **?**. At each epoch the resulting SED is integrated to determine the bolometric light curve of the SN.

Our final sample of 10 SLSNe-I below $z < 0.3$ is presented within Table 2, alongside the fit B, P and τ_m values to the magnetar model outlined above.

3.3.3   Templates

At present, there are few existing samples of SLSN-I spectrophotometric templates, largely as a result of the extreme diversity exhibited within this spectroscopic subclass, both in photometric and spectroscopic evolution.

Therefore for simplicity, we chose to create our template light curves using a parametric model capable of replicating the general form of a SLSN-I event, neglecting the small scale behaviours often present within the main light curve which may be indicative of multiple energy sources (e.g. **?**), as these features do not significantly

Table 1. The derived physical properties of the magnetar models applied to the light curves of low redshift SLSNe.

SN name	z	P_spin (ms)	B ($10^{14}G$)	τ_M (days)
PTF09as	0.1867	19.99	30.00	10.26
PTF09cnd	0.2584	4.53	2.43	14.62
PTF10aagc	0.2067	14.18	25.18	11.12
SN2011kg	0.1924	9.71	8.40	14.25
PTF12dam	0.1073	9.80	2.40	14.45
LSQ14mo	0.253	9.26	8.50	13.86
SN2010gx	0.2297	7.73	6.68	13.59
SN2011ke	0.1428	6.50	10.31	12.60
SN2012il	0.175	13.84	12.44	14.72
SN2015bn	0.1136	3.57	2.90	15.52

affect the detectability of any prospective SLSNe-I event in the survey. We therefore chose to generate our template light curves using a magnetar model, which we detail below.

Models of magnetar spin-down have been found previously to be capable of replicating the broad photometric properties of a large number of SLSN-I light curves (i.e. rise, peak luminosity, slow decline) (**????**), and whilst there remains some debate as to whether the magnetar model alone is able to fully replicate the photometric behaviour of *all* SLSNe-I **[REFS]**, it provides a framework from within which a 'typical' SLSNe light curve may be generated. We therefore adopt the magnetar model of **?**, and as per **?**, we also include a time dependant trapping coefficient introduced by **?** to account for the late-time behaviour of the light curve;

$$L_\mathrm{SN}(t) = \left(1 - \exp\left(\frac{9\kappa M_{ej}^2}{40\pi E_k}t^{-2}\right)\right) \times e^{-(t/\tau_\mathrm{m})^2}$$

$$2\int_0^{t/\tau_\mathrm{m}}\left(\int 4.9\times10^{46}\left(\frac{B}{10^{14}\,\mathrm{G}}\right)^2\left(\frac{P}{\mathrm{ms}}\right)^{-4}\frac{1}{(1+t/\tau_\mathrm{p})^2}\right)$$

$$e^{(t'/\tau_\mathrm{m})^2}\frac{dt'}{\tau_\mathrm{m}}\,\mathrm{erg\,s^{-1}}, \quad (3)$$

where B and P are the magnetic field strength and period of the magnetar respectively, τ_p is the spin down timescale of the magnetar, and τ_m is the diffusion timescale, which under the assumption of uniform ejecta density, can be expressed in terms of the mass, M_ej, opacity, κ, and kinetic energy, E_k of the ejecta. We assume an explosion energy of 10^{51} erg and a hydrogen-free ejecta with an opacity of $\kappa = 0.1$ cm^{2}g^{-1}.

We therefore generate our prospective SLSNe-I light curves by varying values for our three free parameters; namely B, P and τ_m. To determine the range of possible values these parameters may take (thus the final parameter space being sampled), we first fit this magnetar model to the light curves of a representative sample of SLSNe-I.

3.3.4   Generating SLSN Light Curve Templates

To avoid generating 'non SLSNe-I-like' light curves from our magnetar model, we chose to create template light curves based upon magnetars contained within a parameter space which encloses all the fitted magnetar properties of our low-redshift SLSN-I sample. We determine this parameter space using a Khachiyan algorithm (**??**) to determine the smallest volume which contains all of our
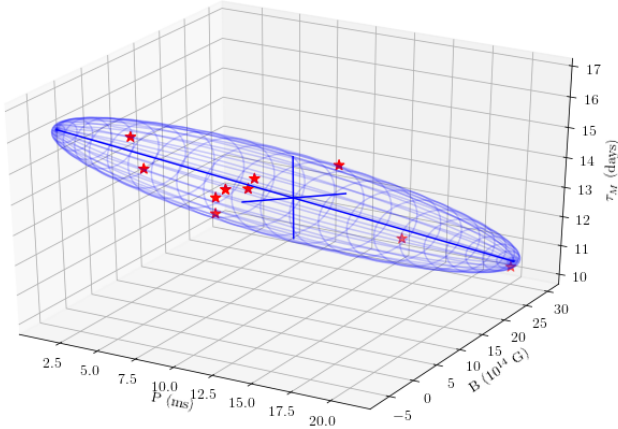
Figure 1. The τ_M-B$_{14}$-P$_{ms}$ magnetar parameter space determined for our low-z SLSNe sample. Need to find way to block out unphysical values in mesh plot!

fitted magnetars. We may then draw templates from fixed combinations of magnetar properties contained in coordinates within this ellipsoidal parameter space. Given the small number of objects used to define this parameter space, we perform jackknife resampling to confirm the determined ellipsoid is not skewed by outlying points, and find our ellipsoid fit to be optimal for the sample. We visualise this final parameter space in Figure 1. However, given the ellipsoidal nature of this parameter space, some of the values enclosed within it are unphysical. We therefore exclude all magnetar combinations containing unphysical values when generating our template light curves.

We finally create a library of template PTF *R*-band light curves using the possible magnetars contained within our defined parameter space. We assume a UV absorbed black body as the underlying SED, and generate observer-frame light curves over all redshifts within the range 0.001< z <0.2, using a redshift bin size of 0.001.

4 THE SUPERNOVA SAMPLE

This section details the construction of both our CCSN and SLSN sample. Our primary obstacle is the classification of transients into the relevant sub-types. To alleviate this our sub-survey parameters were designed to encapsulate times when PTF achieved a regular cadence and high spectroscopic classification efficiency. to minimise the misclassification of SNe and hence contaminants in the final sample. We first describe our light curve coverage cuts and discuss the details of our search for both spectroscopically confirmed as photometrically identified candidates. Again, we stress that any cuts we enforce our real SNe must also be applied to simulated objects later in the analysis.

4.1 Light-curve coverage cuts

The cuts described here are primarily designed to maximise the probability that PTF would have spectroscopically classified the transient. In this regard, we adopt some of the choices made by **?** in their construction of a SN Ia sample. Our coverage cuts are:

- There must be at least four epochs on which the supernova is detected in any 70 sliding window across the survey;
- An object is considered detected if the RB score ≥0.07 (**?**);

- These four epochs must be separated by ≥12 h;

These cuts were applied to the real-time difference-imaging photometry[1] obtained during the PTF survey operation and formed the foundation of our spectroscopic and photometric search for objects.

4.2 The core-collapse sample

We now turn our attention to the construction of the CCSN sample. Our first decision was to set a maxium redshift for an object to be included in our sample. This was set at z≤0.035 and was motivated by ensuring that, at this distance, the fainter end of the CCSN luminosity function Put a citation: Li 2011was above the detection limit of PTF (m ~21.5). We then defined the sky area and date range over which to perform a search of real CCSNe. It is this part of the analysis where PTF presents itself as one of the more unique supernova hunting experiments. Other surveys, such as SDSS-SN cite SDSS, SNLS, or DES, typically adopt a supernova observing strategy involving regular cadenced imaging of a fixed area of the sky. This naturally sets the survey volume for the supernovae, and consequently provides the boundaries for any simulations that aim to replicate the survey operation. PTF was different and performed an evolving search strategy that changed through the lifetime of the survey. To alleviate the complications of searching and simulating a varying footprint, we established 9 areas across 2010–2012 that PTF regularly observed so that we could model each as a distinct sub-survey. These areas were selected through a visual inspection of the PTF fields and were unbiased by the SN distribution on the sky. The parameterization of our sub-survey footprints are listed in Table XX and visualized in Figure XX. We then searched the PTF data to find SN candidates within these sub-surveys and we present our findings in the following sections.

4.2.1 Spectroscopically confirmed CCSN

The spectroscopic follow-up campaign for the PTF survey was performed at several facilities and on a range of instruments. The majority of spectra were taken with the Double Spectrograph on the Palomar 200 inch telescope cite Oke and gunn 82, the Keck 10 m telescope using the Low-resolution Imaging Spectrometer cite LIRS; Oke 1995, the ISIS spectrograph on the 4.2 m William Herschel Telescope, and the Lick Observatory Shane 3 m telescope with the Kast souble spectrograph Mill and Stone 1993.

Events were classified shortly after spectra were obtained using both visual inspection and through the automated classifers SNID Blondin 2007and Superfit Howell 2005. Core-collapse SNe were classified into their various sub-types based on their prominent spectral features (for an overview see; Fillipenko 1997?); Type II (strong H lines), IIb (strong H and He lines), IIn (narrow H), Ib (no H, strong He lines), and Ic (no H or He lines). Additionally, events were classified as SN Ic-BL based on their similarities to, namely, SN 1998bw and SN 2002ap. Furthermore, our Type II events were not sub-divided further into light curve evolution driven categories (IIP/L groups), although we do distinguish Type IIb events as they are believed to originate from a stripped progenitor e.g. Chornock 2010, find more.

Table 2. PTF CCSN photometric candidates

ptfname	ra	dec	redshift
PTF12bvf	177.75691	20.399901	0.022
PTF12gfx	240.413968	16.310245	0.029

We collated a sample of spectroscopically confirmed objects that met our spectroscopic definition of a CCSN, were detected in our sub-surveys, and passed the minimum light curve coverage cuts. In total we found 84 SNe (60 Type II, 24 SESNe) and present these objects in Table XX.

4.2.2 *Photometrically Identified CCSNe*

Due to the limited spectroscopic follow-up resources avaliable to any sky survey, it is enevitable that some SNe will only be identifable through their photometric evolution. Finding these missed events required a search of the PTF transient data base containing $\sim$ 48000 unique candidate objects. This database not only contains SNe, but also a variety of other transient phenomena, such as variable stars and activatae galatic nuclei. Additionally, a large contaminant of non-atrophysical events comes from spurious detections caused by subtraction artefacts.

We begin by applying our strict light curve quality cuts from Section 4.1 and sub-survey parameters from TableXX to reduce the number of potential PTF SN candidates to 987. Most of these objects, however, have been spectroscopically typed and removing those with a definitive classification reduces our candidate sample size to 20. We note that if the object was spectroscopically observed and the classification was unclear we retained the object in our prelimnary sample. These final candidates were cross matched to the SDSS galaxy catalogues and visually inspected to confirm no host misidentification cite sullivan and guptaand in the event of a galaxy redshift we rejected objects with $z_{host}>0.035$. This resulted in three objects that warranted further investigation; PTF12bvf, PTF12cxz, PTF12gfx. We were able to cross-match PTF12cxz with a known SN-imposter candidate later identified in 2014 (**?**)

5   RATE SIMULATION

In this Section we describe our method of calculating the SLSN-I rate in the PTF data. The complexities of calculating supernova rates in survey data are amplified in PTF due to the large observing footprint, variable cadence, and rarity of SLSN-I. To calculate the rate we considered adopting an "efficiency weighting" approach (e.g. **??**) where individual objects are weighted according to the results of a survey simulation. Whilst this method was effective at calculating the SN Ia rate in PTF, **?** required strict data quality cuts in a regularly cadenced domain that only a sub-set of SNe Ia met (N=90). This methodology was justified as it reduced the systematic uncertainties associated with poor quality data, without sacrificing much of the statistical relevance of their sample size. This is something we are unwilling to do as our SLSN-I sample is small to begin with.

We, therefore, adopt and extend a Monte-Carlo simulation approach, similar to **?** and **?**, to estimate the SLSN-I rate. Within the Monte-Carlo simulation an intrinsic volumetric rate (r_{input}) is assumed and used to calculate the number of template light curves to enter the simulation. The template properties are drawn from the input parameter distributions described in Section 1. We then trial different values of r_{input} to build a probability distribution of cases when the simulation output sample is equal in size to the PTF observed sample size ($N_{output} = N_{observed}$).

When calculating any rate, careful consideration must be taken to account for observational biases within the simulation. Our observational detection efficiencies are taken from **?**. As part of the analysis around 7 million artificial point sources were inserted into real observations, this characterised the PTF transient detection pipeline as a function of several key observational properties (source magnitude, seeing, sky background, limiting magnitude, host surface brightness). Ultimately, these detection efficiencies describe the probability that, on any given night during the survey, PTF would have detected an event.

Building on these principles, our method for calculating the volumetric SLSN-I rate proceeds as follows. We first define the sky area and redshift range over which PTF would have been sensitive to SLSNe. Unlike other PTF rates analyses (**??**), we do not sub-divide the sky into smaller well-controlled 'sub-surveys' with a regular cadence. This is because the long duration of SLSN light curves makes them less susceptible to cadence variations. We, therefore, simulate SLSNe over a $\sim$30,000 deg^2 total footprint (Θ_{obs}) (The 30,000deg simulation is 'id=2' in the database) across 3 years of operation from 2010–2012 (T_{obs}). We are unable to perform light curve simulations in data taken in 2009 due to the unreliable nature of the recovery efficiencies during the survey's first few months of operation. We set the upper limit for a simulated object to be z=0.2 following our sample definition in Section Write about the sample.

5.1   SLSN-I Rate

In this Section we present the SLSN-I volumteric rate and discuss the associated uncertainties with this result. The small size of our SLSN sample (N=10) necessarily dictates that our final result is statistics limited. The advantage of our Monte-Carlo simulation technique is the intuitive interpretation of our uncertainties Humble brag alert.

We first generate a probability density function (PDF) for the rates that produced $N_{observed} = 10$ observed SLSNe. This is not the final probability distribution as the number of SNe occurring in a given time-span is described by a Poisson process. To capture this natural variation in counting statistics we weight subsequent PDFs assuming $N_{observed} = (0, 1, 2, \dots)$ following

$$\omega_i(i; \lambda = 10) = e^{-\lambda}\frac{\lambda^i}{i!} \text{ for } i = 0, 1, 2, \dots \qquad (4)$$

where ω_i is the weight factor, i is the number of SNe observed, and λ is the most probable value.

[Chris to finish....]

We measure a final rate of 49^{+28}_{-18} SLSN-I events yr^{-1} Gpc^{-3} at $z = 0.2$. This is consistent with the measurement of (**?**) at similar redshift ($z = 0.17$). In Fig. **??**, we compare the PTF SLSN rate measurement with other published values taken from the literature (e.g. (**????**)) as a function of redshift alongside the cosmic star-formation history normalised to our well-constrained PTF SLSN rate measurement (SFH; see **?**). As expected from progenitor models, the evolution of the SLSNe rate roughly traces the evolution of star-formation throughout cosmic time, although alone this evolution is not enough to distinguish between progenitor masses beyond the $\sim$8 M$_\odot$ progenitor divide between thermonuclear and core-collapse progenitors.
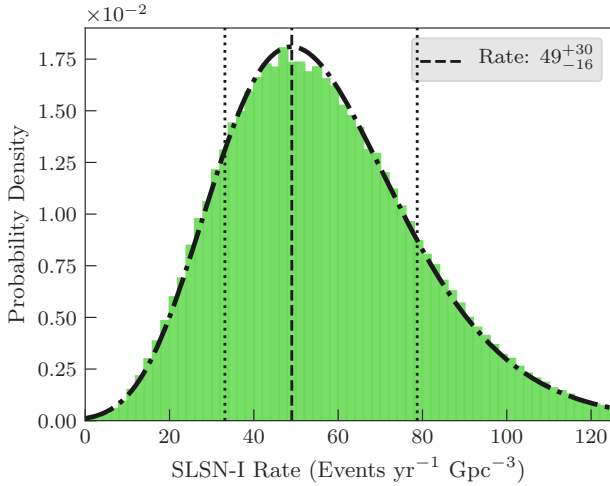
Figure 2. The SLSN-I rate probability distribution

The majority of models for SLSN production reply upon the collapse of single, massive stars, although exactly how massive these progenitors need to be is still uncertain. Even within particular explosion paradigms, the mass of the progenitor can vary as a result of subtle tweaks in the pre-explosion assumptions [**CITE SOME SHIT!**]. Furthermore, the driving environmental properties attributed to the production of a SLSN progenitor over that another core collapse event are difficult to disentangle, be it low-metallicity environments or intensley star forming regions. This is particularly difficult to do in the low-redshift Universie (where the majority of SLSN hosts have identified and studied), as the majority of cosmic star formation in the local Universe is tied up in small, low mass star-bursting galaxies [**REFS**].

Rates provide one way in which we can break the degeneracy between host star formation properties and metallicity. By comparing the ratio of rates of SLSNe to those of other core collapse transients across different redshifts (under the assumption of a constant IMF), we may begin to establish whether any evolution in this ratio is reflected in global galaxy evolution properties (such as the evolution of mass/metallcity with redshift). **To test this, we estimate the rate of all stripped-envelope SNe (SESNe) in PTF using the templates of Vincenzi et al 2019.**

[THINGS TO DO]

- Take Maria's Ibc R-band templates
- Run templates through PTF rate simulation - get Ibc rate in PTF (actuall numbers; 29 Ics, 19 Ibs over our rate period
- Work out R_{SLSN}/R_{Ibc} for z~0.04 (use Li and Richardson LFs)
- Sanity check –> Does it equal Bazin CCSN rate $\times$ 0.34
- Number of Ibc events from Drout paper OR query PTF database (Chris has access?)
- Use cosmic SFH to work backwards so we can compare R_{SLSN}/R_{Ibc} at z 0.04
- Use literature high-z rates (e.g. Szymon's paper) and literature CCSN rates + some extrapolation from CCSN population fractions to vaguely estimate R_{SLSN}/R_{Ibc} for z~1.0
- Comment on how well constrained estimates of this ratio will give you better constraints on progenitors through it's evolution with z (see upcoming DES rate). Compare evolution to e.g. SFR vs z relationship.

6 SUMMARY

ACKNOWLEDGEMENTS

REFERENCES

Angus C. R., et al., 2018, arXiv e-prints, p. arXiv:1812.04071
Aspvall B., Stone R. E., 1980, Journal of Algorithms, 1, 1
Chatzopoulos E., Wheeler J. C., Couch S. M., 2013, ApJ, 776, 129
Chevalier R. A., Irwin C. M., 2011, ApJ, 729, L6
Cooke J., et al., 2012, Nature, 491, 228
Dessart L., 2019, A&A, 621, A141
Dessart L., Hillier D. J., Waldman R., Livne E., Blondin S., 2012, MNRAS, 426, L76
Frohmaier C., Sullivan M., Nugent P. E., Goldstein D. A., DeRose J., 2017, ApJS, 230, 4
Frohmaier C., Sullivan M., Maguire K., Nugent P., 2018, ApJ, 858, 50
Frohmaier C., et al., 2019, MNRAS, 486, 2308
Hopkins A. M., Beacom J. F., 2006, ApJ, 651, 142
Inserra C., et al., 2013, ApJ, 770, 128
Inserra C., et al., 2018a, A&A, 609, A83
Inserra C., Prajs S., Gutierrez C. P., Angus C., Smith M., Sullivan M., 2018b, ApJ, 854, 175
Inserra C., Prajs S., Gutierrez C. P., Angus C., Smith M., Sullivan M., 2018c, ApJ, 854, 175
Kasen D., Bildsten L., 2010, ApJ, 717, 245
Khachiyan L., 1980, USSR Computational Mathematics and Mathematical Physics, 20, 53
Law N. M., Kulkarni S., Ofek E., Quimby R., Kasliwal M., Palomar Transient Factory Collaboration 2009, in American Astronomical Society Meeting Abstracts #213. p. 469.01
Mazzali P. A., Sullivan M., Pian E., Greiner J., Kann D. A., 2016, MNRAS, 458, 3455
McCrum M., et al., 2015, MNRAS, 448, 1206
Moriya T. J., et al., 2018, preprint, (arXiv:1801.08240)
Nicholl M., et al., 2013, Nature, 502, 346
Nicholl M., Guillochon J., Berger E., 2017, ApJ, 850, 55
Pan Y.-C., et al., 2017, MNRAS, 470, 4241
Perrett K., et al., 2012, AJ, 144, 59
Prajs S., et al., 2017, MNRAS, 464, 3568
Quimby R. M., et al., 2011, Nature, 474, 487
Quimby R. M., Yuan F., Akerlof C., Wheeler J. C., 2013, MNRAS, 431, 912
Smith M., et al., 2017, preprint, (arXiv:1712.04535)
Sorokina E., Blinnikov S., Nomoto K., Quimby R., Tolstov A., 2016, ApJ, 829, 17
Tartaglia L., Pastorello A., Benetti S., Cappellaro E., Tomasella L., Ochner P., Elias-Rosa N., Turatto M., 2014, The Astronomer's Telegram, 5737, 1
Villar V. A., Nicholl M., Berger E., 2018, ApJ, 869, 166
Vincenzi M., Sullivan M., Firth R. E., Gutiérrez C. P., Frohmaier C., Smith M., Angus C., Nichol R. C., 2019, arXiv e-prints, p. arXiv:1908.05228
Wang S. Q., Liu L. D., Dai Z. G., Wang L. J., Wu X. F., 2016, ApJ, 828, 87
Woosley S. E., 2010, ApJ, 719, L204
Woosley S. E., Blinnikov S., Heger A., 2007, Nature, 450, 390
Yan L., et al., 2015, ApJ, 814, 108

APPENDIX A: SOME EXTRA MATERIAL

If you want to present additional material which would interrupt the flow of the main paper, it can be placed in an Appendix which appears after the list of references.

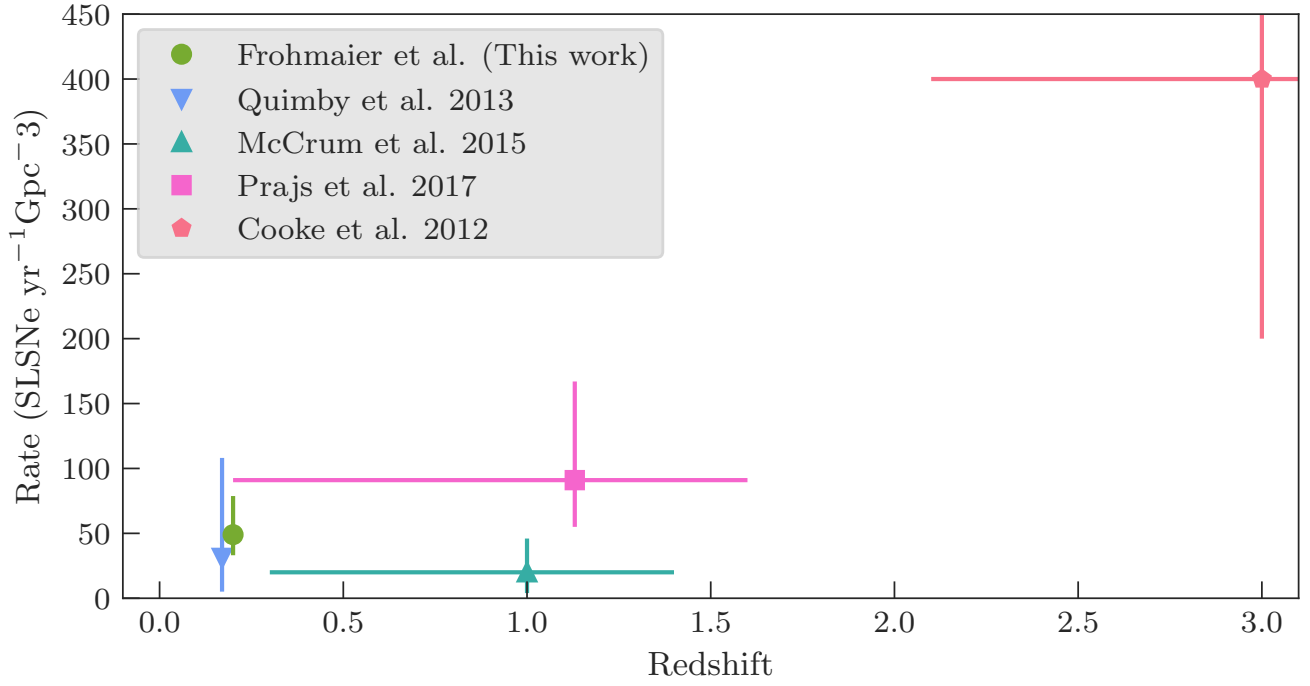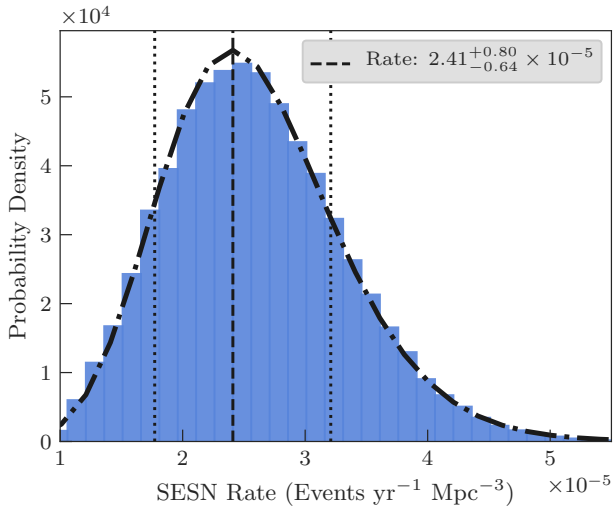This paper has been typeset from a TEX/LATEX file prepared by the author.

Figure 3.

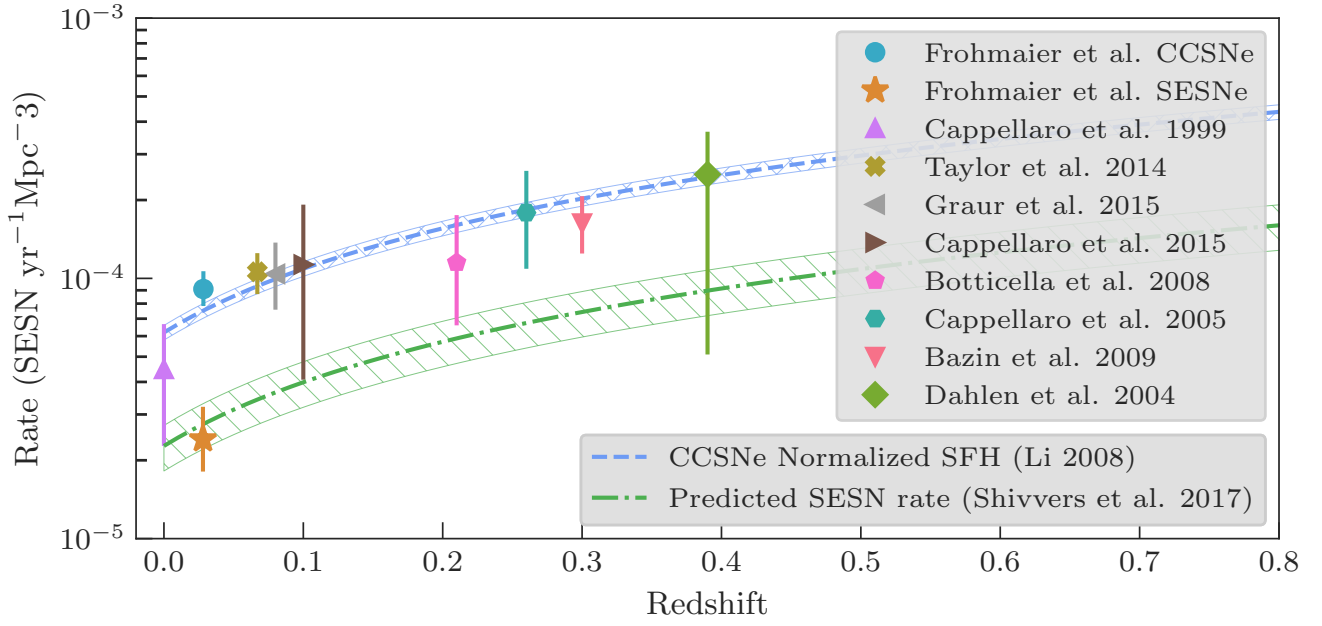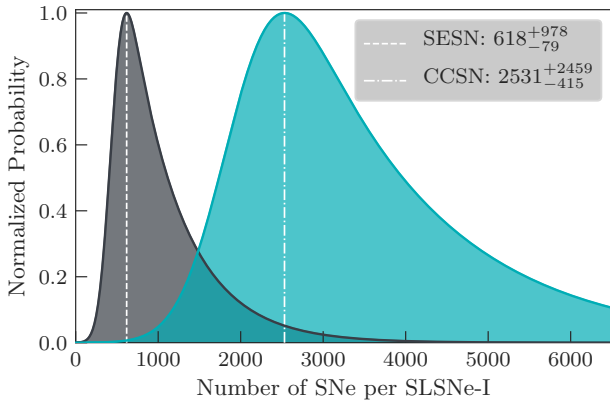**Figure 4.** The SLSN-I rate probability distribution

Figure 5.

Figure 6. The SLSN-I rate probability distribution